Comprehensive characterization of the particulate IVOCs and SVOCs from heavy-duty diesel vehicles using two-dimensional gas chromatography time-of-flight mass spectrometry

Xiao He[1], Xuan Zheng[1*], Shaojun Zhang[2,3], Xuan Wang[4], Ting Chen[1], Xiao Zhang[2], Guanghan Huang[2], Yihuan Cao[2], Liqiang He[2], Xubing Cao[5], Yuan Cheng[5], Shuxiao Wang[2,3], Ye Wu[2,6*]

[1]College of Chemistry and Environmental Engineering, Shenzhen University, Shenzhen 518060, China
[2]School of Environment, State Key Joint Laboratory of Environment Simulation and Pollution Control, Tsinghua University, Beijing 100084, China
[3]State Environmental Protection Key Laboratory of Sources and Control of Air Pollution Complex, Beijing 100084, China
[4]School of Energy and Environment, City University of Hong Kong, Hong Kong SAR, China
[5]State Key Laboratory of Urban Water Resource and Environment, School of Environment, Harbin Institute of Technology, Harbin, 150090, China
[6]Beijing Laboratory of Environmental Frontiers Technologies, Beijing 100084, China

Correspondence to: Xuan Zheng (x-zheng11@szu.edu.cn), Ye Wu (ywu@mail.tsinghua.edu.cn)

Atmospheric
Chemistry
and Physics
Discussions

16 **Abstract.**

17 Tailpipe emissions from three heavy-duty diesel vehicles (HDDVs), complying with varying emission standards

18 and installed with diverse aftertreatment technologies, are collected at a certified chassis dynamometer laboratory.

19 The HDDV-emitted intermediate-volatility and semi-volatile organic compound (I/SVOC) emission and the gas-

20 particle partitioning of the I/SVOCs are investigated. Over four thousand compounds are identified and grouped

21 into twenty-one categories. The dominant compound groups of particulate I/SVOCs are alkanes and phenolic

22 compounds. For HDDVs without aftertreatment devices, i.e., diesel oxidation catalyst (DOC) and diesel

23 particulate filter (DPF), the emitted I/SVOCs partition dramatically into the gas phase (accounting for ~ 93% of

24 the total I/SVOC mass), with a few exceptional categories: hopane, 4-ring polycyclic aromatic hydrocarbons

25 (PAH_{4rings}), and PAH_{5rings}. For HDDVs with DPF and DOC, the particulate fractions are reduced to a negligible

26 level, i.e., less than 2%. Nevertheless, 50% of the total 2-ring PAH mass is detected in the particle phase, which

27 is much higher than the high-molecular-weight PAHs, arising from the positive sampling artifact of quartz filter

28 absorbing organic vapours. The positive sampling artifact of quartz filter absorbing organic vapours is clearly

29 observed and uncertainties are discussed and quantified. Particulate I/SVOCs at low-speed, middle-speed, and

30 high-speed phases are collected and analysed separately. EF distribution of the speciated OA on a two-dimensional

31 volatility basis set (2D-VBS) space reveals that the fractions of OA with O:C (oxygen to carbon) ratio > 0.3 (0.4,

32 0.5) are 18.2% (11.5%, 9.5%), 23% (15.4%, 13.6%), and 29.1% (20.6%, 19.1%) at low-speed, middle-speed, and

33 high-speed stages. The results help to resolve the complex organic mixtures and trace the evolution of OA.

1. Introduction

34

35   The chemical composition of fine particle (particulate matter with aerodynamic diameter less than 2.5 micrometre,

36   $PM_{2.5}$) varies both temporally and spatially. Unlike the inorganic portion that has been well studied, the

37   characterization of organic aerosol, which takes up a major faction of $PM_{2.5}$ mass is yet to achieve (He et al., 2018;

38   Kundu et al., 2010). Nevertheless, the elevated $PM_{2.5}$ concentrations have been widely recognized to be associated

39   with enhanced mortality by epidemiologic studies (Franklin et al., 2008; Tecer et al., 2008; Pope et al., 2004;

40   Dockery, 2001; Laden et al., 2006). For example, exposures to polycyclic aromatic hydrocarbons (PAHs) and the

41   derivatives through inhalation, ingestion, and dermal contact are associated with an increased risk of cancer

42   (Durant et al., 1996; Umbuzeiro et al., 2008).

43   Once emitted into the atmosphere, the volatile organic compounds (VOCs), intermediate-volatility and semi-

44   volatile organic compounds (I/SVOCs) are subject to sequences of chemical and physical evolutions to form

45   secondary organic aerosol (SOA) (Alier et al., 2013; Paasonen et al., 2016; Wang et al., 2006; Stewart et al., 2021a;

46   Stewart et al., 2021b). I/SVOCs span a wide range of volatility and partition dynamically between the gas and

47   particle phases (Alam et al., 2019; Presto et al., 2009). The term effective saturation concentration (C^*, $\mu g\ m^{-3}$) is

48   frequently used to categorize IVOCs ($10^3 < C^* < 10^6\ \mu g\ m^{-3}$), SVOCs ($10^{-1} < C^* < 10^3\ \mu g\ m^{-3}$), and low

49   volatility organic compounds LVOCs ($C^* < 10^{-1}\ \mu g\ m^{-3}$) (Gentner et al., 2012). Diesel vehicle exhaust has

50   contributed significantly to the emission of VOCs, IVOCs, SVOCs, and PM on both global and regional scales

51   (Huang et al., 2015; Liu et al., 2021; Ridley et al., 2018). The abundant emission of the precursors and the dynamic

52   interactions under atmospheric conditions impose significant impacts on climate change and huma health (Luo et

53   al., 2022; Poorfakhraei et al., 2017). In view of such importance, the quantitative characterization of the vehicular

54   organic components, spanning the whole volatility range, is highly needed. While on-road vehicle emitted VOCs

55   have been well speciated and accurately quantified, regardless of fuel type, vehicle type, ignition system, and

56   driving condition, the determination of IVOCs and SVOCs is far from adequate (Kawashima et al., 2006; Gentner

57   et al., 2009).

58   The accurate quantification of I/SVOCs, which composes of thousands of individual compounds, remains a great

59   challenge (Stewart et al., 2021b). They are frequently reported as a few compound categories and leave the

60   majority being unresolved complex mixtures (UCMs) (Qi et al., 2019; Zhao et al., 2014). For instance, alkanes

61   (including *n*-alkanes, *i*-alkanes, and cyclic alkanes) are found to be the dominant fraction in I/SVOCs, contributing

62   to over 60% of total mass, followed by oxygenated and aromatic species (Alam et al., 2019; Lu et al., 2018; He

63   et al., 2022). Crucial structural information, e.g., carbon skeletons and chemical active moieties, is notably missing.

64   The knowledge of structural information at molecular level helps to give a more comprehensive description of the

65   chemical evolution of I/SVOCs from mobile sources and better predict the SOA formation (Chen et al., 2019;

66   Kleindienst et al., 2012; He et al., 2020; Tkacic et al., 2012). Besides, the molecular level composition alters the

67   optical properties of the OA significantly (Li et al., 2018; Li et al., 2021; Harvey et al., 2016).

68   The gas-particle (g-p) partitioning of vehicle emitted I/SVOCs is determined by the mutual effects of intrinsic

69   nature of the organics, e.g., the liquid vapor pressure, and the environmental conditions, e.g., temperature, bulk

70   OA concentration, and heterogeneous reactions (Lu et al., 2018; Sitaras et al., 2004; Chen et al., 2010; Liu et al.,

71   2015). The scenarios of g-p partitioning of vehicle emissions are described by different vehicle types or driving

72   conditions, and limited compound categories are reported (Lu et al., 2018; May et al., 2013a, b). The lacking of

73   phase distribution by chemical speciation biases the SOA model prediction and hinders a full understanding of

74 chemical fate of vehicle emissions (Li et al., 2018; Grieshop et al., 2007). For example, Zhao et al. (2013) reported

75 the g-p partitioning of individual organic species using a thermal desorption aerosol gas chromatography (TAG)

76 instrument and found that contribution of oxygenated compounds to SOA can be substantially increased through

77 g-p partitioning. However, a comprehensive characterization of speciated g-p partition of vehicle emission is yet

78 to achieve.

79 Given such significant research gap, particulate I/SVOCs at ascending speed stages are collected and analysed

80 separately. We integrate the targeted and non-targeted analysis to speciate and quantify them. The emission

81 characteristics are explored, and the speciation-by-speciation g-p partitioning is fully addressed. We observe

82 unusual absorption of IVOC vapours to the sampling surface (i.e., quartz filter), and provide a systematic

83 discussion on the sampling artifact/bias on g-p partitioning equilibrium. Particulate I/SVOCs at ascending speed

84 stages are collected and analysed separately. The results clearly demonstrate that the state-of-the-art instruments

85 enable the characterization of the complex organic mixtures and help to trace the evolution of organic aerosol.

86 **2. Materials and methods**

87 **2.1 Vehicles, driving cycles, and sampling**

88 The tailpipe emissions from the three in-use HDDVs are collected at the China Automotive Technology &

89 Research Centre (CATARC) in Tianjin, China. The vehicles are selected to cover a range of aftertreatment

90 technologies. One HDDV (#1) is installed with selective catalytic reduction (SCR) system and two HDDVs (#2

91 and #3) are installed with SCR, diesel oxidation catalyst (DOC), and diesel particulate filter (DPF). The recruited

92 HDDVs are modelled in year of 2016, 2020, and 2020, respectively and the gross weight are 18.7 t, 25 t, and 25

93 t. Vehicle #1 meets with China IV national emission standard which was implemented back to 2010 and vehicles

94 #2 and #3 comply with China VI national emission standard which come into force in 2021.

95 For each HDDV, they were tested on a chassis dynamometer (AIP-ECDM 72H/2AXLE) and operated over the

96 China heavy-duty commercial vehicle test cycle for heavy trucks (CHTC-HT) cold-start and hot-start driving

97 conditions consecutively. CHTC-HT driving cycle (1800 s) simulates the driving conditions for heavy-duty

98 commercial vehicles in China and is divided into three segments: low-speed (phase one (P1), 342 s), middle-speed

99 (phase two (P2), 988 s), and high-speed (phase three (P3), 470 s). Prior to cold-start, each vehicle was pre-

100 conditioned overnight to cool the engine completely and the time slot between cold-start and hot-start was

101 approximately 10 min. Each test cycle was duplicated for three times.

102 Constant volume sampler (CVS) is equipped with the real-time gas analyser module (MEXA-7400HLE, HORIBA,

103 Japan) to monitor the transient concentration of CO and CO_2. An array of on-line and off-line instruments are

104 deployed to measure the heavy-duty vehicle exhaust in the gas and particle phases. Experimental conditions

105 including temperature, air flow, relative humidity, and pressure and inorganic and organic components are

106 monitored collocated. The details about the sample collection of gaseous I/SVOCs are described elsewhere (He

107 et al., 2022). The particulate I/SVOC collection procedures are given below. Tailpipe emissions from each HDDV

108 is drawn into the CVS system, simultaneously with ambient air which is filtered by high-efficiency particulate air

109 filter. The diluted diesel exhaust is then directed into the second dilution trunk (SDT), where diesel emitted

110 particles are further diluted before entering the PM sampler and being collected by quartz filters. On each test,

111 one 47 mm quartz filter (Grade QM-A, Whatman, UK) is loaded for particle collection. The quartz filters are pre-

112   baked overnight at 550 °C to remove any carbonaceous contamination. The particle sampling probe places at the

113   centre line of the first dilution truck (DT) and 10 times DT inner diameter downstream the emission pipeline to

114   guarantee thorough mixing. The air flows, temperature and humidity control, and dilution ratios within the whole

115   sampling system follow the stipulations of the China VI emission standard (2018). The average temperature in

116   the sampling train is 47 $\pm$ 5 °C. Field blank samples are collected collocated at the upstream of the emission

117   pipeline. The experiment diagram to collect gaseous and particulate emissions and the position of gas monitors

118   are shown in Figure S1.

119   **2.2 Sample treatment and chemical analysis**

120   A total of 36 filter samples plus 3 field blanks were collected and subjected to the determination of I/SVOCs. A

121   precious portion of 1 cm^2 (1 cm $\times$ 1 cm) was removed from the quartz filter and cut into strips before placing

122   into the thermal desorption (TD) tube. 2 μL deuterated internal standard (IS) mixing solution was spiked onto the

123   strips through a mild N_2 blow (CSLR, Markes International). The list of IS species is shown in the supporting

124   information (S1). The TD tubes were placed into an automated thermal desorption system (TD100-xr, Markes

125   International), which is connected to a two-dimensional gas chromatograph (GC $\times$ GC) (Agilent 7890B, Agilent

126   Technologies) coupled with a time-of-flight mass spectrometer (ToF-MS) (LECO Pegasus4D, LECO

127   Corporation).

128   The TD, GC $\times$ GC, and ToF-MS parameters are similar to those previously published for the measurement of

129   gaseous I/SVOCs (He et al., 2022). Briefly, the TD tubes are heated to 315 °C for 20 min where the I/SVOCs are

130   vaporized gradually and condense at the cold trap which is kept at 25 °C. Next, the trap is heated to 330 °C for 5

131   min and the re-concentrated compounds are purged into the GC column in a split ratio of 8.7:1. The first Rxi-5ms

132   capillary column (30 m $\times$ 0.25 mm $\times$ 0.25 μm, Restek) and the second Rxi-17Sil MS (0.75 m $\times$ 0.25 mm $\times$

133   0.25 μm, Restek) capillary column are installed to separate the analytes. A modulator is deployed to partition the

134   effluents from the 1st column into cryo-focused segments and inject them into the 2nd column, with a modulation

135   time slot of 4 s. The column flow is set at 1.3 mL min^{-1} and GC oven initial temperature at 50 °C for 5 min,

136   increased to 300 °C at 5 °C min^{-1}, and held for another 5 min. The secondary oven and modulator temperature are

137   5 °C and 30 °C higher than the GC oven temperature, respectively. The complete run time is approximately 3900

138   s. The ToF-MS is conducted in electron impact positive (EI +) mode (70 eV) scanning over an m/z range of

139   35−550 amu. The ion source temperature is kept at 250 °C.

140   **2.3 Data analysis**

141   Particulate I/SVOCs are identified and quantified with their respective authentic standards or surrogates using the

142   three-step approach proposed in He et al. (2022). In short, within one GC $\times$ GC chromatogram, for the peaks of

143   which the authentic standards are available, they are accurately identified based on the retention time of respective

144   authentic standards and their mass spectrum and precisely quantified based on the constructed calibration curves.

145   The list of authentic standards is shown in Table S1. Nest, for the peaks of which the authentic standards are not

146   available, they are semi-identified by referring to the elusion sequences and extracting mass spectrum patterns via

147   a self-developed algorithm. The syntax is described in He et al. (2022). Third, for the peaks without clear mass

148   spectrum patterns, they are semi-identified by the physically nearest surrogate within the GC $\times$ GC chromatogram.

149 The surrogate is picked out by iterating through all the authentic standards using the self-developed data

150 processing program and comparing the first retention time (RT_1) and second retention time (RT_2) intervals.

151 Basically, thousands of peaks are identified and grouped into twenty-one categories. The classified particulate

152 I/SVOCs include alkane, alkene, cycloalkane, hopane, 2-ring PAHs, 3-ring PAHs, 4-ring $PAHs_{202}$, 4-ring

153 $PAHs_{228}$, 5-ring PAHs, biphenyl & acenaphthene, acid, phenol benzylic alcohol, aliphatic alcohol ether,

154 aliphatic ketone ester, benzylic ketone ester, Nitros, C_2 alkyl benzene, C_3 alkyl benzene, C_4 alkyl benzene, C_5

155 alkyl benzene, and C_6 alkyl benzene.

156 **2.4 Calculation of emission factors (EFs)**

157 Particulate I/SVOC EFs are determined using the following equation by assuming that the CO_2 and CO are the

158 dominant combustion products of diesel fuel.

159
$$EF = (\frac{\Delta I/SVOCs}{V_S} \times \frac{V_{cvs} \times 10^6}{\Delta[CO_2] \times M_C/M_{CO_2} + \Delta[CO] \times M_C/M_{CO}})w_C$$

160 where EF is the emission factor of particulate I/SVOCs (mg·kg·fuel^{-1}); $\Delta I/SVOCs$ is the mass deposited on the

161 quartz filter in the CVS (mg), which is corrected for the background contamination measured on the field blanks

162 and column bleedings; $\Delta[CO_2]$ and $\Delta[CO]$ are the background-corrected CO_2 and CO masses (mg), respectively;

163 M_{CO_2}, M_{CO}, and M_C are the molar weight of CO_2, CO, and C atom; V_{cvs} and V_S are the air flow monitored in the

164 CVS and particle sampling trunk (L min^{-1}); w_C is the mass fraction of carbon (0.86) in the diesel fuel.

165 **3. Results and discussion**

166 **3.1 Emission factors and the chemical speciation and of particulate I/SVOCs**

167 Figure 1 shows the speciated emission factor of the HDDV-emitted I/SVOCs in the particle phase. Generally,

168 over four thousand individual peaks are detected within different tailpipe samples and grouped into twenty-one

169 categories after the three-step data treatment procedure. The average HDDV-emitted particulate I/SVOCs EFs of

170 cold-start and hot-start driving cycles are 147.8 and 1.7 mg kg·fuel^{-1} for non-(DPF + DOC) vehicles, 1.6 and 0.9

171 mg kg·fuel^{-1} for (DPF + DOC) vehicles. Substantial removal effect of the aftertreatment devices is confirmed. A

172 category specified EFs for the non-(DOC + DPF) and (DOC + DPF) vehicles are shown in Table S2.

173 In general, alkane is the most abundant species, taking up 22-63% of the total particulate I/SVOCs followed by

174 2-ring PAHs (20-33%) and phenol benzylic alcohols (14-17%). The sum of the three categories accounts for more

175 than 75% of the total particulate I/SVOCs. The EF of alkane derived from non-(DOC + DPF) vehicles under the

176 cold-start condition averages to 92 mg kg·fuel^{-1}, which is two orders of magnitude higher than that of hot-start

177 cycle and (DOC + DPF) vehicles, as illustrated by the grey squares in Figure 1. Alkene and cycloalkane show

178 commensurate EFs, with the average values of 2.4 and 1.8 mg kg·fuel^{-1} for cold-start and 0.04 and 0.05 mg kg·fuel-

179 ^{1} for hot-start driving cycle for non-(DOC + DPF) vehicles, accounting for minor parts of the total particulate

180 I/SVOCs. The emission of the two species is further reduced after the installation of aftertreatment devices.

181 2-ring to 5-ring PAHs are frequently detected in particulate I/SVOCs, which is different from the gaseous

182 I/SVOCs that only 2-ring to 4-ring PAHs were observed (He et al., 2022). The averaged EFs of PAH subgroup

183 vary significantly. For example, for non-(DOC + DPF) vehicles operated under cold-start driving condition, 2-

184 ring PAHs are detected at abundant concentration of 33.8 mg kg·fuel^{-1}, whereas 3-ring, 4-ring, and 5-ring PAHs

Atmospheric
Chemistry
and Physics
Discussions

Open Access

EGU

185   are detected at much less concentration of 1.5, 1.3, and 0.8 mg kg·fuel^{-1}, respectively. It was reported that 16

186   priority PAHs listed by the United States Environment Protection Agency accounted for a minor fraction of the

187   total PAH mass and the non-targeted analysis has highlighted the significance of the un-resolved PAHs (An et al.,

188   2022; Chen et al., 2022). The two isomers, biphenyl and acenaphthene, contribute least (less than 0.2%) within

189   the PAH subgroup, which is consistent with previous findings (Hazarika et al., 2019).

190   Oxygenated compounds, including phenol benzylic alcohols, aliphatic ketones, benzylic ketones, and acids are

191   routinely detected. The EFs sum up to over 7% of the total mass. Aliphatic alcohols are observed to be abundant

192   in the gas phase but not detectable in particulate I/SVOCs (He et al., 2022). The installation of DPF and DOC

193   reduces the emission of oxygenates by over 93-99%. For instance, the EF of benzylic alcohols of non-(DOC +

194   DPF) vehicles is 2.83 mg kg·fuel^{-1} whereas that of (DOC + DPF) vehicles is 0.15 mg kg·fuel^{-1}.

195   The EF of Nitros is measured to be 0.4 mg kg·fuel^{-1} on average, taking up of 1.6% of the total mass. The

196   installation of DPF and DOC reduces the emission of Nitros by over 95%, from 1.08 mg kg·fuel^{-1} to 0.05 mg

197   kg·fuel^{-1}. Mono-aromatic compounds, which were measured to take up over 10% of the gaseous I/SVOCs, are

198   negligible constituents in the particle phase (He et al., 2022).

199
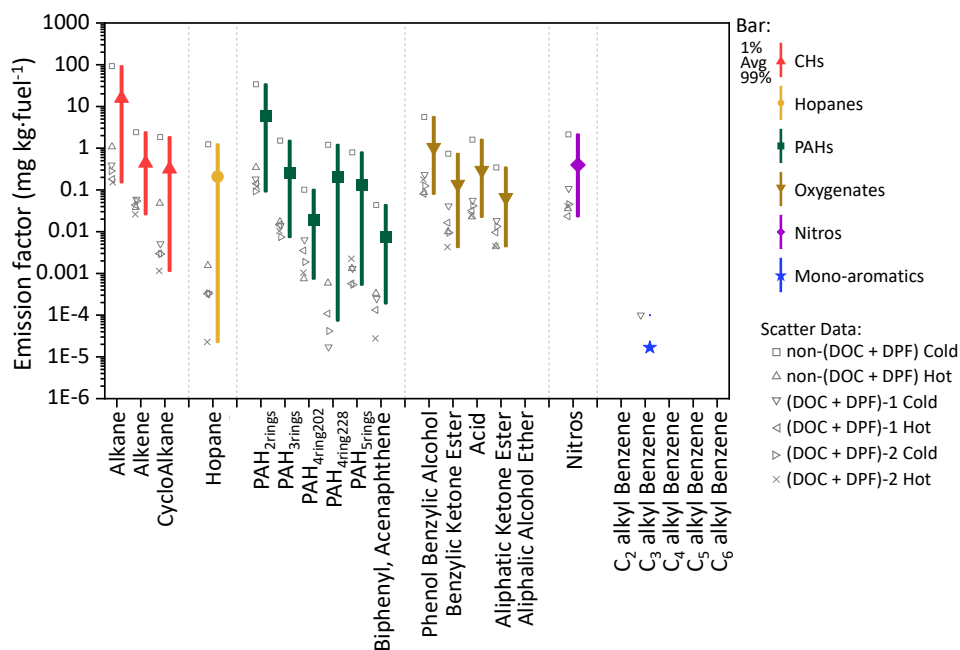
Figure 1. The measured emission factor (mg kg·fuel⁻¹) of the twenty-one categories of the HDDV-emitted I/SVOCs in the particle phase. Coloured-bars and coloured-scatters/shaped-scatters represent different organic species and driving cycles. The square dots in the middle of each bar denote the average value and the lower and upper boundaries of the bar denote the 1% and 99% percentile of the values.

Atmospheric
Chemistry
and Physics
Discussions

Open Access

EGU

204   **3.2 Volatility distribution of the speciated I/SVOCs and the comparison between cold and hot starts**

205   Figure 2 displays the volatility distribution of the speciated I/SVOCs under the cold-start and hot-start driving

206   cycles for non-(DOC + DPF) vehicles and (DOC + DPF) vehicles. Inserted pie charts illustrate the color-labeled

207   mass contributions of each compound category. The absolute values of I/SVOC EFs distributed in each volatility

208   and O:C bin are summarized in Tables S3 - S8. The calculation of the saturation mass concentration is presented

209   in the supporting information (S4). The volatility distributions among the four test conditions, i.e., cold-start non-

210   (DOC + DPF) ($C_{wo}AT$), hot-start non-(DOC + DPF) ($H_{wo}AT$), cold-start (DOC + DPF) ($C_{wi}AT$), and hot-start

211   (DOC + DPF) ($H_{wi}AT$), do not vary much except the two peaks at $\log_{10}C^* = -4$ μg m^{-3} and $\log_{10}C^* = -3$ μg m^{-3}

212   under $C_{wo}AT$ and $H_{wo}AT$ (Figure 2a and 2b). The abnormal abundant emissions indicate intensive incomplete

213   combustion processes, especially under cold-start condition. The high emissions at the low volatility end vanish

214   after the installation of DOC and DPF (Figure 2a vs. Figure 2c, Figure 2b vs. Figure 2d), revealing that the

215   aftertreatment devices eliminate the low volatility compounds, mostly alkanes, efficiently. Great environment

216   benefits are thereby expected with the advancing of the aftertreatment technologies.

217   The majority of particulate I/SVOCs distribute in the volatility range of $\log_{10}C^* = 1$ to 8 μg m^{-3} while the specified

218   compound categories distribute differently and could be classified into three groups. First, alkanes are observed

219   within the whole volatility range at abundant level. Second, hopanes, PAH$_{4rings}$, and PAH$_{5rings}$ reside in the

220   volatility range of $\log_{10}C^* \leq -2$ μg m^{-3} dominantly. For example, about 44% of hopane mass are measured in the

221   volatility bin of $\log_{10}C^* = -3$ μg m^{-3}. Third, light molecular weight PAHs, oxygenated compounds, and Nitros

222   present in the volatility range of $\log_{10}C^* \geq 2$ μg m^{-3} substantially. For example, phenol benzylic alcohols, the

223   most abundant oxygenated compounds observed in particulate I/SVOCs, partition into the high volatile range

224   entirely.

225   The mass fractions of O-I/SVOCs under the cold-start and hot-start driving cycles in the gas and particle phases

226   are shown in Figure S3. The impacts of O-I/SVOCs on SOA formation are complex. On one hand, the formation

227   potential of oxidized components is lower than that of hydrocarbons, for example alkane (Chacon-Madrid and

228   Donahue, 2011; Donahue et al., 2011; Ziemann, 2011). On the other hand, the increasing O:C ratio adds

229   fragmentation on the carbon skeleton which would facilitate SOA formation (Donahue et al., 2012; Kroll et al.,

230   2009). An increasing trend of mass fraction of particulate O-I/SVOCs from low volatility end to high volatility

231   end is clearly demonstrated whereas a bimodal pattern of gaseous O-I/SVOCs is observed. The gaseous O-

232   I/SVOCs were divided into two major groups with one group peaking in the volatility range of $\log_{10}C^* = 4$ to 8

233   μg m^{-3} and another group prevailing in the volatility range of $\log_{10}C^* = -2$ to 3 μg m^{-3}. The two groups possess

234   different chemical structures and functional groups. They were fully addressed in previous work and will not be

235   repeated here (He et al., 2022). By contrast, one compound category, phenol benzylic alcohols, dominates in the

236   particulate O-I/SVOC. The mass fraction of phenol benzylic alcohols is 5% and 6% for non-(DOC + DPF)

237   vehicles under cold-start and hot-start conditions, respectively. The mass ratio increases to 26% and 22% for

238   (DOC + DPF) vehicles. It contributes significantly to the total mass in the high volatility range of $\log_{10}C^* = 6$ to

239   8 μg m^{-3}.
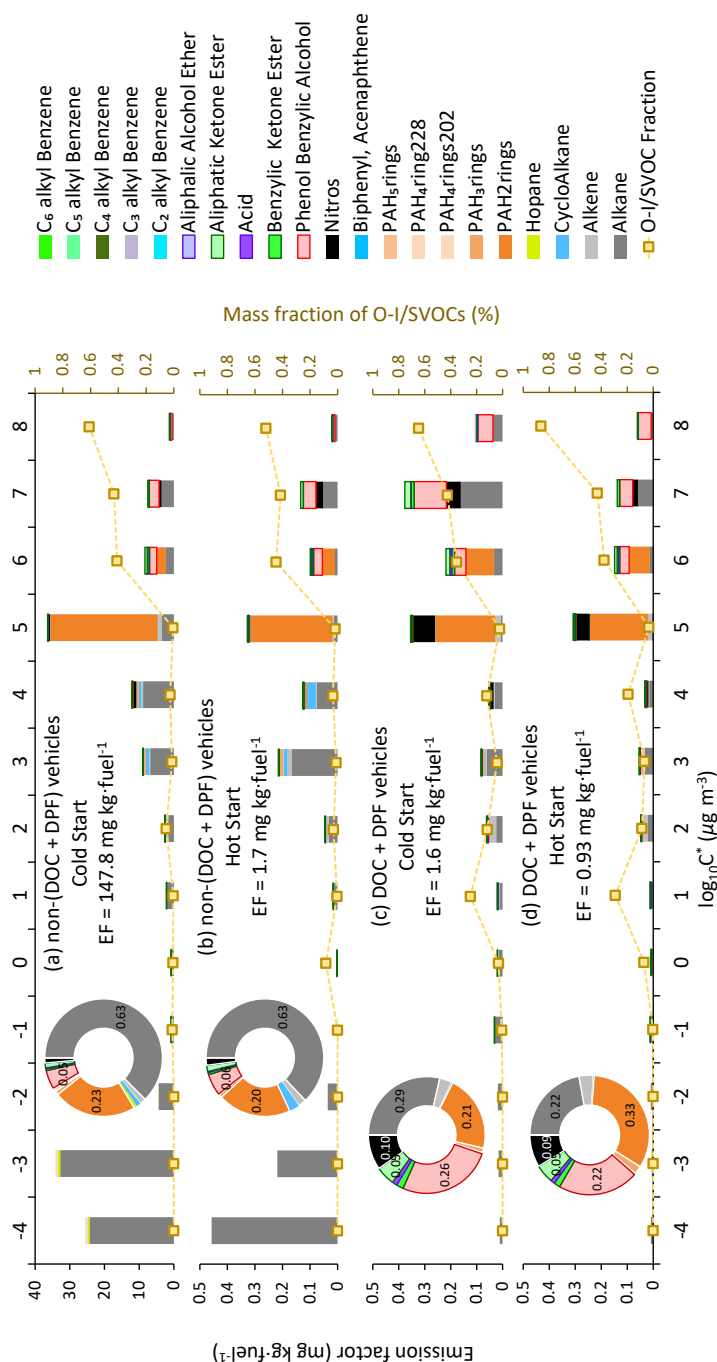
Figure 2. EFs of particulate I/SVOCs under the cold-start and hot-start driving cycles. Different coloured bars represent different compound categories. Mass fraction of the O-I/SVOCs, indicated by the scattered squares, is scaled by the right axis. Embed pie charts are the mass fractions of different compound categories, and the numbers show the mass contributions of the top few species.

245 **3.3 The EF distribution of particulate I/SVOCs**

246 Figure 3 and Figure 4 display the EF distribution of the speciated particulate I/SVOCs on a two-dimensional

247 volatility basis set (2D-VBS) space of P1, P2, P3, and whole (W_cold and W_hot) driving cycles. The absolute

248 values of I/SVOC EFs distributed in each volatility and O:C bin are summarized in Tables S3 – S12.

249 Distinct distribution patterns are observed between different speed stages. For non-(DPF + DOC) vehicles, peak

250 signals of P1 are detected at low volatility and O:C ratio bins, i.e., $\log_{10}C^* = -3$ to -4 μg m^{-3} and O:C < 0.3

251 whereas those of P2 and P3 are measured at $\log_{10}C^* = 3$ to 7 μg m^{-3} and the fraction of I/SVOCs with higher O:C

252 ratio increases, especially at high-speed stage (P3). For example, the fractions of I/SVOC with O:C > 0.3 (0.4,

253 0.5) are 18.4% (10.2%, 7.0%), 13.4% (8.3%, 7.6%), and 25.3% (19.4%, 18.6%) for P1, P2, and P3 stages. The

254 fraction of I/SVOCs with higher O:C ratio decreases rapidly to less than 10% for low and middle-speed stages,

255 contrast with which the fraction remains at comparable level for high-speed stage. The emission characteristics of

256 the whole driving cycle combine the patterns of the separate speed phases, and a bimodal trend is observed as

257 displayed in Figure 5d and 5e.

258 After the installation of aftertreatment devices, the peak signals of P1 are detected at high volatility bins, i.e.,

259 $\log_{10}C^* = 3$ to 7 μg m^{-3} and low O:C range. In comparison with non-(DPF + DOC) vehicles, the EF volatility

260 distribution of P1 resembles that of P2 and P3 whereas the fraction of I/SVOCs with higher O:C ratio of P1 is still

261 lower than that of P2 and P3. The fractions of I/SVOC with O:C > 0.3 (0.4, 0.5) are 18.1% (12.1%, 10.8%), 27.8%

262 (18.9%, 16.6%), and 31.0% (21.2%, 19.3%) for P1, P2, and P3 stages, considering that the O:C ratio of the bulk

263 organic species varies from 0.25 to 0.5.

264 Comparing the EF distribution of I/SVOCs emitted by different types of vehicles under the same driving

265 conditions, as shown in Figure 5, it is clearly demonstrated that the aftertreatment devices favour the formation

266 of I/SVOCs with higher oxidation state. DOC promotes the oxidation of exhaust gases and the organics filtrated

267 by DPF by oxygen and the I/SVOCs with O:C > 0.3 (0.4, 0.5) under the W_cold condition increase from 0.13 to

268 0.35 (0.11 to 0.18, 0.08 to 0.16) after the equipment of these aftertreatment devices. The respective fractions under

269 W_hot condition increase from 0.18 to 0.26, 0.09 to 0.25, and 0.07 to 0.23, respectively.

270
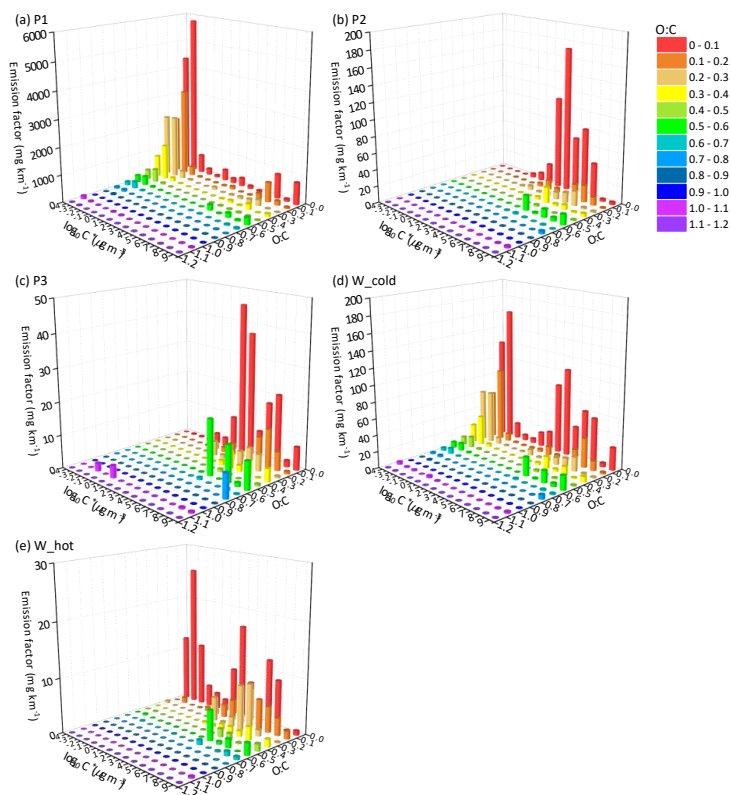
Figure 3. Emission factor distribution of the speciated I/SVOCs of non-(DPF + DOC) vehicles on a 2D-VBS space of (a) low-speed stage (P1), (b) middle-speed stage (P2), (c) high-speed stage (P3), (d) whole (W_cold), and whole (W_hot) driving cycles. Different colours indicate different O:C ratios segmented into 12 bins: 0-0.1, 0.1-0.2, 0.2-0.3, 0.3-0.4, 0.4-0.5, 0.5-0.6, 0.6-0.7, 0.7-0.8, 0.8-0.9, 0.9-1.0, and 1.1-1.2.
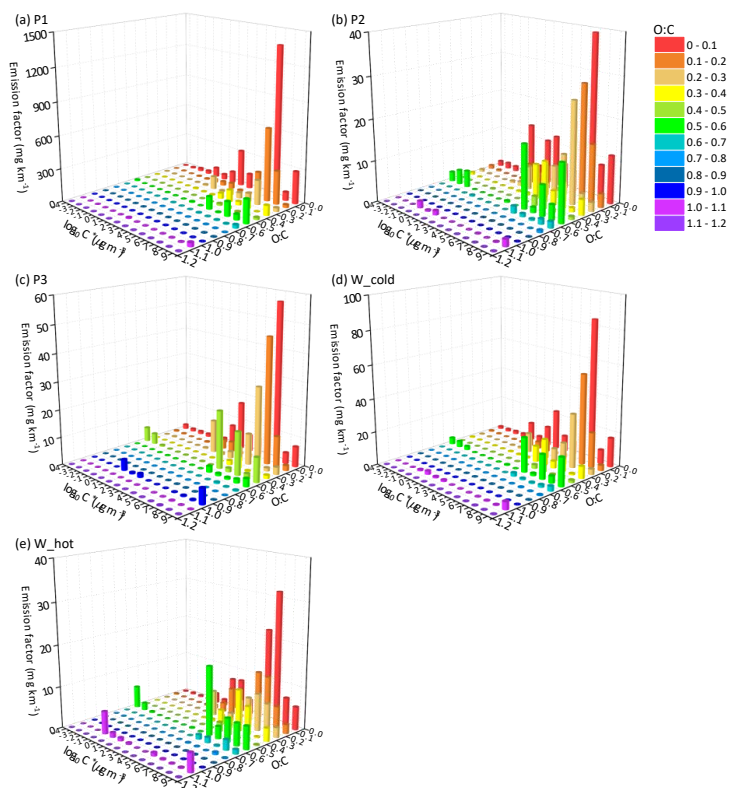
Figure 4. Emission factor distribution of the speciated I/SVOCs of (DPF + DOC) vehicles on a 2D-VBS space of (a) low-speed stage (P1), (b) middle-speed stage (P2), (c) high-speed stage (P3), (d) whole (W_cold), and whole (W_hot) driving cycles. Different colours indicate different O:C ratios segmented into 12 bins: 0-0.1, 0.1-0.2, 0.2-0.3, 0.3-0.4, 0.4-0.5, 0.5-0.6, 0.6-0.7, 0.7-0.8, 0.8-0.9, 0.9-1.0, and 1.1-1.2.
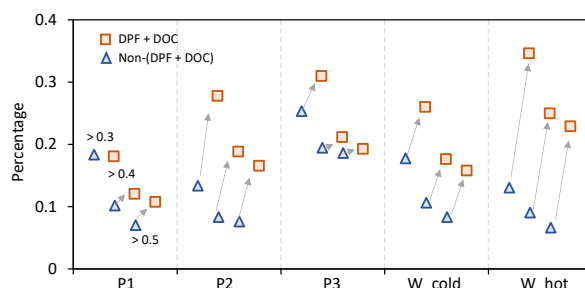
Figure 5. The increment of I/SVOC with O:C > 0.3, 0.4, and 0.5 from non-(DPF + DOC) to (DPF + DOC) vehicles under low-speed stage (P1), middle-speed stage (P2), high-speed stage (P3), and whole (W_cold, W_cold) driving cycles.

3.4 Gas particle partitioning of HDDV-emitted I/SVOCs and the uncertainties/artifacts

Figure 6 shows the g-p partitioning by different compound categories. Generally, the I/SVOCs partition predominantly to the gas phase, with a few exception categories: hopanes, 2ring, 4-ring, and 5-ring PAHs. Distinct patterns are observed between vehicles with and without DPF and DOC. For example, the particle phase contributes 7.4% to the total I/SVOC mass for non-(DPF + DOC) vehicles, whereas it accounts for less than 0.2% for (DPF + DOC) vehicles. Similar mass distributions are observed for alkanes, 3-ring PAHs, and oxygenated species, which confirms the high particle removal efficiency of the aftertreatment devices. The monoaromatic compounds, i.e., C_2-C_6 alkyl-substituted benzenes, are not detected in the particle phase, regardless of the aftertreatment devices. Over 40% 4-ring PAHs partition to the particle phase for non-(DPF + DOC) vehicles and the portion is reduced to less than 0.1% when DPF and DOC systems are installed. The particle fraction of 2-ring PAHs is 57%, whereas that of 3-ring, 4-ring, and 5-ring PAHs are 8.4%, 43.7%, and 100%, respectively.

The adsorption of gaseous I/SVOCs onto filters causes negative biases in the measured gas phase concentration and positive artifacts in the measured particle phase concentration (Turpin et al., 1994). Compared with quartz filter, which absorbs vapours significantly (May et al., 2013a), teflon has small surface area and is relatively inert. However, the vapor loss to the Teflon surface has long been a concern, especially in smog chamber community (Hu and Kamens, 2007; Mohr et al., 2009). Moreover, the OA concentration in the tailpipe is orders of magnitude higher than that in the ambient air even after the dilution in the CVS system. With such high OA loadings, the g-p partitioning shift to the particle phase. Although inevitable, the bias should be closely watched. For example, the sampling tube is short enough (less than 50 cm) to minimize the g-p conversion in the sampling system (the residence time is less than the time scale to reach g-p equilibrium) (Saleh et al., 2013) and Teflon filter is deployed instead of a quartz filter. Good news is that there will be a significant pressure drop before and after the Teflon filter, and the lower pressure behind the Teflon drives the g-p portioning to the gas phase, which offsets the vapor loss by some extent (Turpin et al., 1994).

We then quantify the sampling artifacts. As shown in Figure 7, the particle mass fraction increases gradually from $\log_{10}C^* = 8$ µg m^{-3} to $\log_{10}C^* = -4$ µg m^{-3}. Similar trends were observed previously (Lu et al., 2018). There is a peak in the volatility range of $\log_{10}C^* = 3$ to 7 µg m^{-3} when the particle mass fraction fluctuates around 10% (Figure 7a). The particle fraction decreases to less than 1% between $\log_{10}C^* = -1$ to 2 µg m^{-3}. It is highly likely that the peak reflects the sampling artifacts originated from the vapor loss to the quartz filter. DOC component oxidizes and removes the exhausted gases efficiently, as a consequent of which the sampling artifacts is reduced, i.e., 10% to 1%. The vapor loss occurs in a certain volatility range instead of the whole volatility range, e.g.,

313    $\log_{10}C^* = 3$ to 7 μg m^{-3} and dominant in $\log_{10}C^* = 5$ μg m^{-3} bin in this study. The gaseous IVOCs in $\log_{10}C^* = 8$

314   μg m^{-3} bin may be too volatile to be absorbed by quartz filter. For non-(DPF + DOC) vehicles, the particle fraction

315   approximates 1% at $\log_{10}C^* = 8$ μg m^{-3} and $\log_{10}C^* = 2$ μg m^{-3} bins (the volatility bins adjacent to the bins with

316   sampling artifacts). If we assume that the particle fraction baseline is 1% during the volatility range of $\log_{10}C^* =$

317   2 to 8 μg m^{-3}, we may deduce that the vapor loss to quartz filter results in a negative bias to the gaseous I/SVOCs

318   mass with an upper limit of 9% and approximate 90% of the particulate I/SVOCs result from sampling artifacts

319   in the volatility range of $\log_{10}C^* = 3$ to 7 μg m^{-3}. It is also worth mentioning that the absorption bias varies

320   significantly for different compound categories. For example, substantial 2-ring PAHs are detected in the particle

321   phase whereas no notable sampling artifacts are observed for phenol benzylic alcohols and benzylic ketone esters.
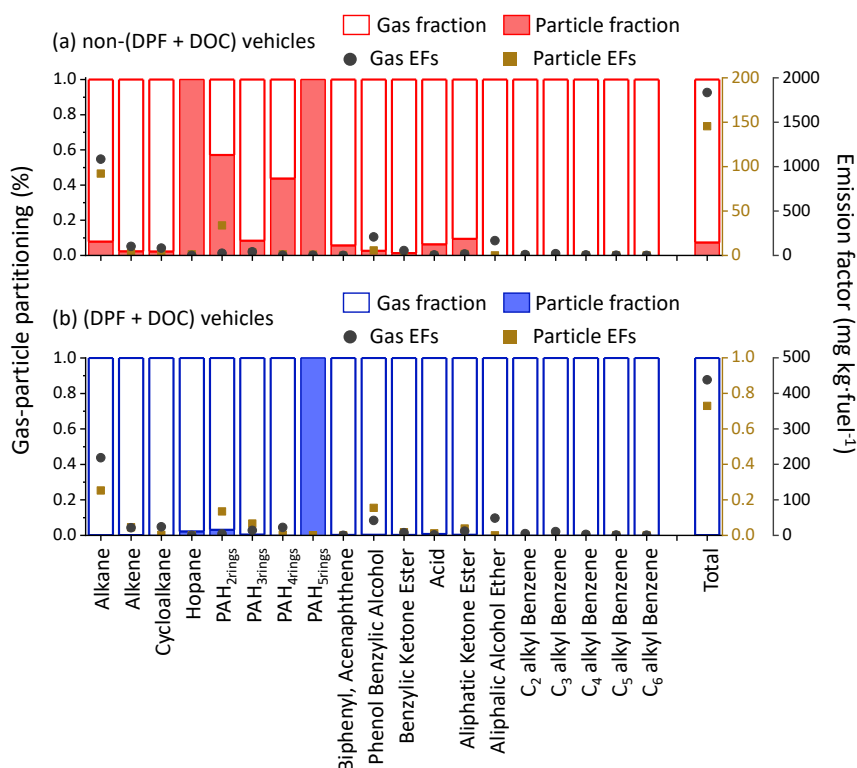
Figure 6. The gas-particle partitioning of speciated I/SVOCs emitted from (a) non-(DPF + DOC) vehicles and (b) (DPF + DOC) vehicles. The hollow and filled columns represent the gas and particle fraction, respectively. The grey dots and brown squares represent the emission factors of the gaseous and particulate I/SVOCs.
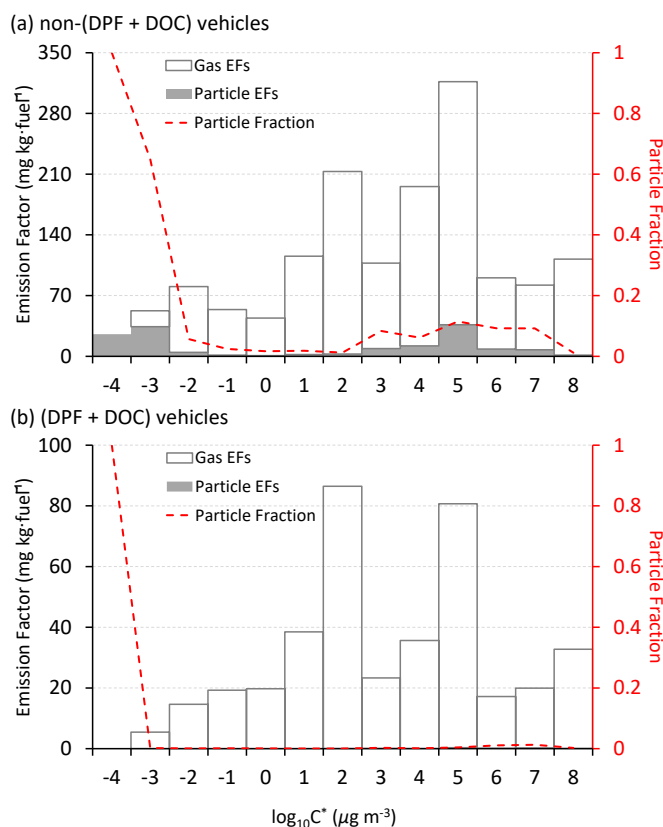
Figure 7. The emission factors of gaseous and particulate I/SVOCs (hollow and filled stack columns) and the particle mass fraction (red dashed line) in each volatility bin computed from (a) non-(DPF + DOC) vehicles and (b) (DPF + DOC) vehicles.

4. Conclusions

Chassis dynamometer tests of HDDVs complying with multiple emission standards are conducted to characterize the particulate I/SVOCs. Thousands of induvial organic compounds are detected and classified, where alkanes and phenolic compounds are observed to be the most abundant groups. The species-by-species g-p partitioning of the I/SVOCs are discussed separately for vehicles with and without aftertreatment devices. Generally, the I/SVOCs partition to the gas phase dominantly. For non-(DPF + DOC) vehicles, the gaseous I/SVOCs account for ~ 93% of the total mass, except for hopane, PAH_{4rings}, and PAH_{5rings}. For (DPF + DOC) vehicles, the particulate fraction of I/SVOCs are further reduced to less than 2%. Sampling artifacts of quartz filter absorbing organic vapours are confirmed by the abnormal high signal of 2-ring PAHs, and the uncertainties are discussed thoroughly. Speciation information is highly needed to better predict the thermodynamics of oxidation chemistry. The application of GC × GC-ToF-MS and self-constructed data processing programs achieve the detailed identification and quantification of particulate I/SVOCs. Although not resolved at molecular level, the speciated information enables us to better characterize the emission scenarios and guides the implementation of control

Atmospheric
Chemistry
and Physics
Discussions
Open Access
EGU

343 strategies in the future. This approach is versatile and could be applied not only to vehicle emissions but also to

344 other significant sources prevailing in typical environments, e.g., biomass burning and ship emissions, as well as

345 ambient samples collected at receptor sites. Putting the speciated I/SVOC data into atmospheric models and

346 emission inventories, we expect a significantly improved estimation of SOA locally and globally.

347 **Data availability**

348 The measurement data used in this study are available in the data repository:

349 https://figshare.com/articles/dataset/Emission_factor_summary_the_g-

350 p_partition_and_the_removal_effciency_xlsm/19994603.

351 **Author contribution:**

352 Xiao He: Conceptualization, Methodology, Validation, Investigation, Formal Analysis, Writing-Original Draft,

353 Data Curation, Visualization, Funding Acquisition. Xuan Zheng: Project Management, Validation, Writing-

354 Review & Editing, Funding Acquisition. Shaojun Zhang: Validation, Writing-Review & Editing. Xuan Wang:

355 Validation, Writing-Review & Editing. Ting Chen: Investigation. Xiao Zhang: Investigation. Guanghan Huang:

356 Investigation. Yihuan Cao: Investigation. Liqiang He: Investigation. Xubing Cao: Investigation. Yuan Cheng:

357 Investigation. Shuxiao Wang: Resources, Writing-Review & Editing, Funding Acquisition. Ye Wu: Resources,

358 Supervision, Funding Acquisition

359 **Declaration of Competing Interest**

360 The authors declare no competing financial interests.

361 **Acknowledgements**

References

Limits and measurement methods for emissions from diesel fuelled heavy-duty vehicles (CHINA VI), 2018.

Alam, M. S., Zeraati-Rezaei, S., Xu, H., and Harrison, R. M.: Characterization of Gas and Particulate Phase Organic Emissions (C9-C37) from a Diesel Engine and the Effect of Abatement Devices, Environ. Sci. Technol., 53, 11345-11352, 10.1021/acs.est.9b03053, 2019.

Alier, M., van Drooge, B. L., Dall'Osto, M., Querol, X., Grimalt, J. O., and Tauler, R.: Source apportionment of submicron organic aerosol at an urban background and a road site in Barcelona (Spain) during SAPUSS, Atmospheric Chemistry and Physics, 13, 10353-10371, 2013.

An, Z., Li, X., Yuan, Y., Duan, F., and Jiang, J.: Large contribution of non-priority PAHs in atmospheric fine particles: Insights from time-resolved measurement and nontarget analysis, Environ. Int., 163, 107193, 10.1016/j.envint.2022.107193, 2022.

Chacon-Madrid, H. J. and Donahue, N. M.: Fragmentation vs. functionalization: chemical aging and organic aerosol formation, Atmos. Chem. Phys., 11, 10553-10563, 10.5194/acp-11-10553-2011, 2011.

Chen, J. J., Jakober, C., Clegg, S., and Kleeman, M. J.: Theoretical versus Observed Gas-Particle Partitioning of Carbonyl Emissions from Motor Vehicles, J. Air Waste Manage. Assoc., 60, 1237-1244, 10.3155/1047-3289.60.10.1237, 2010.

Chen, T., Zheng, X., He, X., You, Y., Huang, G. H., Cao, Y. H., He, L. Q., and Wu, Y.: Comprehensive characterization of polycyclic aromatic hydrocarbon emissions from heavy-duty diesel vehicles utilizing GC × GC-ToF-MS, Sci. Total Environ., 155127, https://doi.org/10.1016/j.scitotenv.2022.155127, 2022.

Chen, T. Z., Liu, Y. C., Liu, C. G., Liu, J., Chu, B. W., and He, H.: Important role of aromatic hydrocarbons in SOA formation from unburned gasoline vapor, Atmos. Environ., 201, 101-109, 10.1016/j.atmosenv.2019.01.001, 2019.

Dockery, D. W.: Epidemiologic evidence of cardiovascular effects of particulate air pollution, Environ. Health Perspect., 109, 483-486, Doi 10.2307/3454657, 2001.

Donahue, N. M., Epstein, S. A., Pandis, S. N., and Robinson, A. L.: A two-dimensional volatility basis set: 1. organic-aerosol mixing thermodynamics, Atmos. Chem. Phys., 11, 3303-3318, 10.5194/acp-11-3303-2011, 2011.

Donahue, N. M., Henry, K. M., Mentel, T. F., Kiendler-Scharr, A., Spindler, C., Bohn, B., Brauers, T., Dorn, H. P., Fuchs, H., Tillmann, R., Wahner, A., Saathoff, H., Naumann, K. H., Mohler, O., Leisner, T., Muller, L., Reinnig, M. C., Hoffmann, T., Salo, K., Hallquist, M., Frosch, M., Bilde, M., Tritscher, T., Barmet, P., Praplan, A. P., DeCarlo, P. F., Dommen, J., Prevot, A. S. H., and Baltensperger, U.: Aging of biogenic secondary organic aerosol via gas-phase OH radical reactions, Proc. Natl. Acad. Sci. U.S.A., 109, 13503-13508, 10.1073/pnas.1115186109, 2012.

Durant, J. L., Busby, W. F., Lafleur, A. L., Penman, B. W., and Crespi, C. L.: Human cell mutagenicity of oxygenated, nitrated and unsubstituted polycyclic aromatic hydrocarbons associated with urban aerosols, Mutat Res-Genet Tox, 371, 123-157, 1996.

Franklin, M., Koutrakis, P., and Schwartz, J.: The role of particle composition on the association between PM2.5 and mortality, Epidemiology, 19, 680-689, DOI 10.1097/EDE.0b013e3181812bb7, 2008.

Gentner, D. R., Harley, R. A., Miller, A. M., and Goldstein, A. H.: Diurnal and Seasonal Variability of Gasoline-Related Volatile Organic Compound Emissions in Riverside, California, Environ. Sci. Technol., 43, 4247-4252, 10.1021/es9006228, 2009.

Gentner, D. R., Isaacman, G., Worton, D. R., Chan, A. W. H., Dallmann, T. R., Davis, L., Liu, S., Day, D. A., Russell, L. M., Wilson, K. R., Weber, R., Guha, A., Harley, R. A., and Goldstein, A. H.: Elucidating secondary organic aerosol from diesel and gasoline vehicles through detailed characterization of organic carbon emissions, Proc. Natl. Acad. Sci. U.S.A., 109, 18318-18323, 10.1073/pnas.1212272109, 2012.

Grieshop, A. P., Donahue, N. M., and Robinson, A. L.: Is the gas-particle partitioning in alpha-pinene secondary organic aerosol reversible?, Geophys. Res. Lett., 34, 10.1029/2007GL029987, 2007.

Harvey, R. M., Bateman, A. P., Jain, S., Li, Y. J., Martin, M., and Petrucci, G. A.: Optical Properties of Secondary Organic Aerosol from cis-3-Hexenol and cis-3-Hexenyl Acetate: Effect of Chemical Composition, Humidity, and Phase, Environ. Sci. Technol., 50, 4997-5006, 10.1021/acs.est.6b00625, 2016.

Hazarika, N., Das, A., Kamal, V., Anwar, K., Srivastava, A., and Jain, V. K.: Particle phase PAHs in the atmosphere of Delhi-NCR: With spatial distribution, source characterization and risk approximation, Atmos. Environ., 200, 329-342, 10.1016/j.atmosenv.2018.11.064, 2019.

He, X., Huang, X. H. H., Chow, K. S., Wang, Q., Zhang, T., Wu, D., and Yu, J. Z.: Abundance and Sources of Phthalic Acids, Benzene-Tricarboxylic Acids, and Phenolic Acids in PM2.5 at Urban and Suburban Sites in Southern China, ACS Earth and Space Chemistry, 2, 147-158, 10.1021/acsearthspacechem.7b00131, 2018.

He, X., Zheng, X., Yan, Y., Zhang, S. J., Zhao, B., Wang, X., Huang, G. H., Chen, T., Cao, Y. H., He, L. Q., Chang, X., Wang, S. X., and Wu, Y.: Comprehensive chemical characterization of gaseous I/SVOC emissions from heavy-duty

422   diesel vehicles using two-dimensional gas chromatography time-of-flight mass spectrometry, Environ. Pollut.,
423   305, 119284, 10.1016/j.envpol.2022.119284, 2022.
424   He, X., Wang, Q. Q., Huang, X. H. H., Huang, D. D., Zhou, M., Qiao, L. P., Zhu, S. H., Ma, Y. G., Wang, H. L., Li, L.,
425   Huang, C., Xu, W., Worsnop, D. R., Goldstein, A. H., and Yu, J. Z.: Hourly measurements of organic molecular
426   markers in urban Shanghai, China: Observation of enhanced formation of secondary organic aerosol during
427   particulate matter episodic periods, Atmos. Environ., 240, 1-14, 2020.
428   Hu, D. and Kamens, R. M.: Evaluation of the UNC toluene-SOA mechanism with respect to other chamber studies
429   and key model parameters, Atmos. Environ., 41, 6465-6477, 10.1016/j.atmosenv.2007.04.026, 2007.
430   Huang, C., Wang, H. L., Li, L., Wang, Q., Lu, Q., de Gouw, J. A., Zhou, M., Jing, S. A., Lu, J., and Chen, C. H.: VOC
431   species and emission inventory from vehicles and their SOA formation potentials estimation in Shanghai, China,
432   Atmos. Chem. Phys., 15, 11081-11096, 10.5194/acp-15-11081-2015, 2015.
433   Kawashima, H., Minami, S., Hanai, Y., and Fushimi, A.: Volatile organic compound emission factors from roadside
434   measurements, Atmos. Environ., 40, 2301-2312, 10.1016/j.atmosenv.2005.11.044, 2006.
435   Kleindienst, T. E., Jaoui, M., Lewandowski, M., Offenberg, J. H., and Docherty, K. S.: The formation of SOA and
436   chemical tracer compounds from the photooxidation of naphthalene and its methyl analogs in the presence and
437   absence of nitrogen oxides, Atmos. Chem. Phys., 12, 8711-8726, 10.5194/acp-12-8711-2012, 2012.
438   Kroll, J. H., Smith, J. D., Che, D. L., Kessler, S. H., Worsnop, D. R., and Wilson, K. R.: Measurement of fragmentation
439   and functionalization pathways in the heterogeneous oxidation of oxidized organic aerosol, PCCP, 11, 8005-8014,
440   10.1039/b905289e, 2009.
441   Kundu, S., Kawamura, K., Andreae, T. W., Hoffer, A., and Andreae, M. O.: Diurnal variation in the water-soluble
442   inorganic ions, organic carbon and isotopic compositions of total carbon and nitrogen in biomass burning
443   aerosols from the LBA-SMOCC campaign in Rondonia, Brazil, J. Aerosol Sci, 41, 118-133,
444   10.1016/j.jaerosci.2009.08.006, 2010.
445   Laden, F., Schwartz, J., Speizer, F. E., and Dockery, D. W.: Reduction in fine particulate air pollution and mortality
446   - Extended follow-up of the Harvard six cities study, Am. J. Respir. Crit. Care Med., 173, 667-672,
447   10.1164/rccm.200503-443OC, 2006.
448   Li, J. L., Wang, W. G., Li, K., Zhang, W. Y., Peng, C., Liu, M. Y., Chen, Y., Zhou, L., Li, H., and Ge, M. F.: Effect of
449   chemical structure on optical properties of secondary organic aerosols derived from C-12 alkanes, Sci. Total
450   Environ., 751, 141620, 10.1016/j.scitotenv.2020.141620, 2021.
451   Li, K., Li, J. L., Wang, W. G., Li, J. J., Peng, C., Wnag, D., and Ge, M. F.: Effects of Gas-Particle Partitioning on
452   Refractive Index and Chemical Composition of m-Xylene Secondary Organic Aerosol, J. Phys. Chem. A, 122, 3250-
453   3260, 10.1021/acs.jpca.7b12792, 2018.
454   Liu, Y., Gao, Y., Yu, N., Zhang, C., Wang, S., Ma, L., Zhao, J., and Lohmann, R.: Particulate matter, gaseous and
455   particulate polycyclic aromatic hydrocarbons (PAHs) in an urban traffic tunnel of China: Emission from on-road
456   vehicles and gas-particle partitioning, Chemosphere, 134, 52-59, 10.1016/j.chemosphere.2015.03.065, 2015.
457   Liu, Y. X., Li, Y. J., Yuan, Z. B., Wang, H. L., Sha, Q. E., Lou, S. R., Liu, Y. H., Hao, Y. Q., Duan, L. J., Ye, P. L., Zheng, J.
458   Y., Yuan, B., and Shao, M.: Identification of two main origins of intermediate-volatility organic compound
459   emissions from vehicles in China through two-phase simultaneous characterization, Environ. Pollut., 281,
460   117020, 10.1016/j.envpol.2021.117020, 2021.
461   Lu, Q., Zhao, Y., and Robinson, A. L.: Comprehensive organic emission profiles for gasoline, diesel, and gas-
462   turbine engines including intermediate and semi-volatile organic compound emissions, Atmos. Chem. Phys., 18,
463   17637-17654, 10.5194/acp-18-17637-2018, 2018.
464   Luo, Z., Wang, Y., Lv, Z., He, T., Zhao, J., Wang, Y., Gao, F., Zhang, Z., and Liu, H.: Impacts of vehicle emission on
465   air quality and human health in China, Sci. Total Environ., 813, 152655, 10.1016/j.scitotenv.2021.152655, 2022.
466   May, A. A., Presto, A. A., Hennigan, C. J., Nguyen, N. T., Gordon, T. D., and Robinson, A. L.: Gas-Particle
467   Partitioning of Primary Organic Aerosol Emissions: (2) Diesel Vehicles, Environ. Sci. Technol., 47, 8288-8296,
468   10.1021/es400782j, 2013a.
469   May, A. A., Presto, A. A., Hennigan, C. J., Nguyen, N. T., Gordon, T. D., and Robinson, A. L.: Gas-particle
470   partitioning of primary organic aerosol emissions: (1) Gasoline vehicle exhaust, Atmos. Environ., 77, 128-139,
471   10.1016/j.atmosenv.2013.04.060, 2013b.
472   Mohr, C., Huffman, J. A., Cubison, M. J., Aiken, A. C., Docherty, K. S., Kimmel, J. R., Ulbrich, I. M., Hannigan, M.,
473   and Jimenez, J. L.: Characterization of Primary Organic Aerosol Emissions from Meat Cooking, Trash Burning, and
474   Motor Vehicles with High-Resolution Aerosol Mass Spectrometry and Comparison with Ambient and Chamber
475   Observations, Environ. Sci. Technol., 43, 2443-2449, 10.1021/es8011518, 2009.
476   Paasonen, P., Kupiainen, K., Klimont, Z., Visschedijk, A., van der Gon, H. A. C. D., and Amann, M.: Continental
477   anthropogenic primary particle number emissions, Atmospheric Chemistry and Physics, 16, 6823-6840, 2016.

478 Poorfakhraei, A., Tayarani, M., and Rowangould, G.: Evaluating health outcomes from vehicle emissions
479 exposure in the long range regional transportation planning process, J Transp Health, 6, 501-515,
480 10.1016/j.jth.2017.05.177, 2017.
481 Pope, C. A., Burnett, R. T., Thurston, G. D., Thun, M. J., Calle, E. E., Krewski, D., and Godleski, J. J.: Cardiovascular
482 mortality and long-term exposure to particulate air pollution - Epidemiological evidence of general
483 pathophysiological pathways of disease, Circulation, 109, 71-77, 10.1161/01.Cir.0000108927.80044.7f, 2004.
484 Presto, A. A., Miracolo, M. A., Kroll, J. H., Worsnop, D. R., Robinson, A. L., and Donahue, N. M.: Intermediate-
485 Volatility Organic Compounds: A Potential Source of Ambient Oxidized Organic Aerosol, Environ. Sci. Technol.,
486 43, 4744-4749, 10.1021/es803219q, 2009.
487 Qi, L. J., Liu, H., Shen, X. E., Fu, M. L., Huang, F. F., Man, H. Y., Deng, F. Y., Shaikh, A. A., Wang, X. T., Dong, R.,
488 Song, C., and He, K. B.: Intermediate-Volatility Organic Compound Emissions from Nonroad Construction
489 Machinery under Different Operation Modes, Environ. Sci. Technol., 53, 13832-13840, 10.1021/acs.est.9b01316,
490 2019.
491 Ridley, D. A., Heald, C. L., Ridley, K. J., and Kroll, J. H.: Causes and consequences of decreasing atmospheric
492 organic aerosol in the United States, Proc. Natl. Acad. Sci. U.S.A., 115, 290-295, 10.1073/pnas.1700387115, 2018.
493 Saleh, R., Donahue, N. M., and Robinson, A. L.: Time Scales for Gas-Particle Partitioning Equilibration of
494 Secondary Organic Aerosol Formed from Alpha-Pinene Ozonolysis, Environ. Sci. Technol., 47, 5588-5594,
495 10.1021/es400078d, 2013.
496 Sitaras, I. E., Bakeas, E. B., and Siskos, P. A.: Gas/particle partitioning of seven volatile polycyclic aromatic
497 hydrocarbons in a heavy traffic urban area, Sci. Total Environ., 327, 249-264, 10.1016/j.scitotenv.2003.08.022,
498 2004.
499 Stewart, G. J., Nelson, B. S., Drysdale, W. S., Acton, W. J. F., Vaughan, A. R., Hopkins, J. R., Dunmore, R. E., Hewitt,
500 C. N., Nemitz, E., Mullinger, N., Langford, B., Shivani, Reyes-Villegas, E., Gadi, R., Rickard, A. R., Lee, J. D., and
501 Hamilton, J. F.: Sources of non-methane hydrocarbons in surface air in Delhi, India, Faraday Discuss., 226, 409-
502 431, 10.1039/d0fd00087f, 2021a.
503 Stewart, G. J., Acton, W. J. F., Nelson, B. S., Vaughan, A. R., Hopkins, J. R., Arya, R., Mondal, A., Jangirh, R., Ahlawat,
504 S., Yadav, L., Sharma, S. K., Dunmore, R. E., Yunus, S. S. M., Hewitt, C. N., Nemitz, E., Mullinger, N., Gadi, R., Sahu,
505 L. K., Tripathi, N., Rickard, A. R., Lee, J. D., Mandal, T. K., and Hamilton, J. F.: Emissions of non-methane volatile
506 organic compounds from combustion of domestic fuels in Delhi, India, Atmos. Chem. Phys., 21, 2383-2406,
507 10.5194/acp-21-2383-2021, 2021b.
508 Tecer, L. H., Alagha, O., Karaca, F., Tuncel, G., and Eldes, N.: Particulate matter (PM2.5, PM10-2.5, and PM10)
509 and children's hospital admissions for asthma and respiratory diseases: A bidirectional case-crossover study,
510 Journal of Toxicology and Environmental Health-Part a-Current Issues, 71, 512-520,
511 10.1080/15287390801907459, 2008.
512 Tkacik, D. S., Presto, A. A., Donahue, N. M., and Robinson, A. L.: Secondary Organic Aerosol Formation from
513 Intermediate-Volatility Organic Compounds: Cyclic, Linear, and Branched Alkanes, Environ. Sci. Technol., 46,
514 8773-8781, 10.1021/es301112c, 2012.
515 Turpin, B. J., Huntzicker, J. J., and Hering, S. V.: Investigation of Organic Aerosol Sampling Artifacts in the Los-
516 Angeles Basin, Atmos. Environ., 28, 3061-3071, Doi 10.1016/1352-2310(94)00133-6, 1994.
517 Umbuzeiro, G. A., Franco, A., Martins, M. H., Kummrow, F., Carvalho, L., Schmeiser, H. H., Leykauf, J., Stiborova,
518 M., and Claxton, L. D.: Mutagenicity and DNA adduct formation of PAH, nitro-PAH, and oxy-PAH fractions of
519 atmospheric particulate matter from Sao Paulo, Brazil, Mutat Res-Gen Tox En, 652, 72-80, 2008.
520 Wang, X. L., Sato, T., and Xing, B. S.: Size distribution and anthropogenic sources apportionment of airborne
521 trace metals in Kanazawa, Japan, Chemosphere, 65, 2440-2448, 2006.
522 Zhao, Y., Hennigan, C. J., May, A. A., Tkacik, D. S., De Gouw, J. A., Gilman, J. B., Kuster, W. C., Borbon, A., and
523 Robinson, A. L.: Intermediate-Volatility Organic Compounds: A Large Source of Secondary Organic Aerosol,
524 Environ. Sci. Technol., 48, 13743-13750, 10.1021/es5035188, 2014.
525 Zhao, Y. L., Kreisberg, N. M., Worton, D. R., Isaacman, G., Weber, R. J., Liu, S., Day, D. A., Russell, L. M., Markovic,
526 M. Z., VandenBoer, T. C., Murphy, J. G., Hering, S. V., and Goldstein, A. H.: Insights into Secondary Organic
527 Aerosol Formation Mechanisms from Measured Gas/Particle Partitioning of Specific Organic Tracer Compounds,
528 Environ. Sci. Technol., 47, 3781-3787, 10.1021/es304587x, 2013.
529 Ziemann, P. J.: Effects of molecular structure on the chemistry of aerosol formation from the OH-radical-initiated
530 oxidation of alkanes and alkenes, Int. Rev. Phys. Chem., 30, 161-195, 10.1080/0144235x.2010.550728, 2011.